Korea-Australia Rheology Journal
Vol. 21, No. 1, March 2009 pp. 47-58

Numerical description of start-up viscoelastic plane Poiseuille flow

Kwang Sun Park and Young don Kwon*
Department of Chemical Engineering, Sungkyunkwan University, Suwon, Kyunggi-do 440-746, Korea
(Received October 6, 2008; final revision received December 10, 2008)

Abstract

We have investigated the transient behavior of 1D fully developed Poiseuille viscoelastic flow under finite pressure gradient described by the Oldroyd-B and Leonov constitutive equations. For analysis we employ a simple 2nd order discretization scheme such as central difference for space and the Crank-Nicolson for time approximation. For the analysis of the Oldroyd-B model, we also apply the analytical solution, which is obtained again in this work in terms of elementary solution procedure simpler than the previous one (Waters and King, 1970). Both models demonstrate qualitatively similar solutions, but their eventual steady flowrate exhibits noticeable difference due to the absence or presence of shear thinning behavior. In the inertialess flow, the flowrate instantaneously attains a large value corresponding to the Newtonian creeping flow and then decreases to its steady value when the applied pressure gradient is low. However with finite liquid density the flow field shows severe fluctuation even accompanying reversals of flow directions. As the assigned pressure gradient increases, the flowrate achieves its steady value significantly higher than its value during oscillations after quite long period of time. We have also illustrated comparison between 1D and 2D results and possible mechanism of complex 2D flow rearrangement employing a previous solution of finite element computation. In addition, we discuss some mathematical points regarding missing boundary conditions in 2D modeling due to the change of the type of differential equations when varying from inertialess to inertial flow.

Keywords : Leonov model, Oldroyd-B model, Poiseuille flow, flow fluctuation, flow reversal, pressure gradient

1. Introduction

Numerical study of 1D start-up Poiseuille viscoelastic flow presents several consequences in recent years. It may simulate the blood flow along a blood vessel which is time-dependent viscoelastic Poiseuille flow and can be approximately considered axisymmetric, and thus it contains significance in medical science or physiology. In recent years, analysis of time-dependent viscoelastic flow draws our attention due to its industrial importance as well as original scientific concern. Like injection molding, blow molding and thermoforming processes, there are important polymer processing operations that have to be investigated according not to steady flow but to transient flow analysis. When developing a computation code for transient viscoelastic flow simulation, this 1D Poiseuille flow suggests a good starting point, since some basic viscoelastic constitutive equations provide analytical solutions. In this study, we present numerical solutions for the 1D start-up planar Poiseuille flow of the Oldroyd-B and Leonov liquids. Since the analytical solution for the Oldroyd-B model is readily available (Waters and King, 1970), one can estimate the accuracy of approximate solutions by direct comparison of solutions, and therefore this problem proposes a good benchmark test for developing numerical codes.

This problem has already been explored in terms of the finite element method for the Johnson-Segalman fluid by Fyrillas *et al.* (1999), the spectral element method by van Os and Phillips (2004), the finite volume method by Duarte *et al.* (2008), and the finite element/volume method by Sato and Richardson (1994) in order to test their time-dependent computation algorithm, if we mention only a few in this field. Especially Duarte and coworkers (2008) have considered the pulsating Poiseuille flow in addition and its analytical solutions has also been derived.

As previously mentioned, the computing of transient viscoelastic flows becomes more popular due to its industrial and scientific importance and also due to its own possibility recently endowed by the development of high power computers. In these problems, we are again confronted with similar difficulties found in steady flow modeling such as the high Deborah (or Weissenberg) number flow problems exhibited by the loss of evolution and poor mesh convergence. Good review regarding recent development

*Corresponding author: kwon@skku.edu

may be given by Tanner and Xue (2002) and Xue *et al.* (2004).

We in this study also examine the same 1D transient flow problem for 2 types of differential viscoelastic constitutive equations, employing the simplest finite difference method of spatial and the Crank-Nicolson method for temporal discretization. For the Oldroyd-B model, we suggest a simpler procedure of deriving the analytical solution and with it we verify the accuracy of the computation algorithm. In inertial flows, we demonstrate solutions of highly fluctuating flow field for both liquids and also illustrate the possibility of qualitatively different behavior when the applied pressure gradient becomes larger.

2. Equations in 1D time-dependent Poiseuille flow

In order to describe dynamic flow behavior of incompressible fluids, we first require the equation of motion and continuity equation

$$\rho\left(\frac{\partial \mathbf{v}}{\partial t}+\mathbf{v}\cdot\nabla\mathbf{v}\right)=-\nabla p+\nabla\cdot\boldsymbol{\tau},\quad \nabla\cdot\mathbf{v}=0. \tag{1}$$

Here ρ is the density of the liquid, $\mathbf{v}$ the velocity, $\boldsymbol{\tau}$ the extra-stress tensor and p is the pressure. The gravitational force is neglected in the analysis and ∇ is the usual gradient operator in tensor calculus. When kinematic relation of the extra-stress is specified in terms of the constitutive model, the set of governing equations becomes complete for isothermal incompressible viscoelastic flows.

In expressing viscoelastic property of the liquid, the Oldroyd-B and the Leonov constitutive equations (Leonov, 1976) are employed. The differential viscoelastic constitutive equations derived by Oldroyd and Leonov can be written into the following quite general form:

$$\boldsymbol{\tau}=\begin{cases}(1-s)G\mathbf{c}+2\eta s\mathbf{e}\text{: Oldroyd-B model}\\ (1-s)G\left(\frac{I_1}{3}\right)^n\mathbf{c}+2\eta s\mathbf{e}\text{: Leonov model, }\mathbf{e}=\frac{1}{2}(\nabla\mathbf{v}+\nabla\mathbf{v}^T)\end{cases}$$

$$\begin{cases}\frac{d\mathbf{c}}{dt}-\nabla\mathbf{v}^T\cdot\mathbf{c}-\mathbf{c}\cdot\nabla\mathbf{v}+\frac{1}{\theta}(\mathbf{c}-\boldsymbol{\delta})=\mathbf{0}\text{: Oldroyd-B model}\\ \frac{d\mathbf{c}}{dt}-\nabla\mathbf{v}^T\cdot\mathbf{c}-\mathbf{c}\cdot\nabla\mathbf{v}+\frac{1}{2\theta}\left(\mathbf{c}^2+\frac{I_2-I_1}{3}\mathbf{c}-\boldsymbol{\delta}\right)=\mathbf{0}\text{: Leonov model}\end{cases} \tag{2}$$

Here $\mathbf{c}$ of the Leonov model is the recoverable strain tensor that explains elastic strain accumulation in the Finger measure during flow, and in the case of the Oldroyd-B equation it can be similarly interpreted as the elastic strain of the dumbbell if we associate the model with the molecular kinetic theory. $\frac{d\mathbf{c}}{dt}=\frac{\partial\mathbf{c}}{\partial t}+\mathbf{v}\cdot\nabla\mathbf{c}$ is the total time derivative of $\mathbf{c}$, $\frac{d\mathbf{c}}{dt}-\nabla\mathbf{v}^T\cdot\mathbf{c}-\mathbf{c}\cdot\nabla\mathbf{v}$ the upper convected time derivative, G the modulus, θ the relaxation time, $\eta=G\theta$ is the total viscosity that corresponds to the zero-shear viscosity and s is the retardation parameter (ratio of retardation to relaxation time) that specifies the solvent viscosity contribution. The tensor $\mathbf{c}$ reduces to the unit tensor $\boldsymbol{\delta}$ in the stationary state and this also serves as the initial condition in the start-up flow from the rest. In the asymptotic limit of $\theta\to\infty$ with $s=0$ where the material exhibits purely elastic behavior, it becomes the total Finger strain tensor.

$I_1=\mathrm{tr}\mathbf{c}$ and $I_2=\mathrm{tr}\mathbf{c}^{-1}$ for the Leonov model are the basic first and second invariants of $\mathbf{c}$, respectively, and they coincide in planar flows. Due to the characteristic of the Leonov model, the third invariant I_3 satisfies specific incompressibility condition such as $I_3\equiv\det\mathbf{c}=1$. In addition to the linear viscoelastic parameters, it contains a nonlinear constant n ($n>0$), which can be determined from simple shear and uniaxial extensional flow experiments certainly in the nonlinear regime. It controls the strength of shear thinning and extension hardening of the liquid. The total stress tensor is obtained from the elastic potential W based on the Murnaghan's relation. Since the extra-stress is invariant under the addition of arbitrary isotropic terms, when one presents numerical results it may be preferable to use $\boldsymbol{\tau}=(1-s)G\left(\frac{I_1}{3}\right)^n(\mathbf{c}-\boldsymbol{\delta})+2\eta s\mathbf{e}$ instead in order for the stress to vanish in the rest state.

In the case of start-up planar Poiseuille flow ($v_1=v(t,x_2)$, $v_2=v_3=0$), the set of Eqs. (1) and (2) for the Oldroyd-B model reduces to

$$\frac{\partial c_{11}}{\partial t}-2\frac{\partial v}{\partial y}c_{12}+c_{11}-1=0,\ \frac{\partial c_{12}}{\partial t}-\frac{\partial v}{\partial y}+c_{12}=0,\ c_{22}=c_{33}=1,$$
$$c_{13}=c_{23}=0,\ \frac{Re}{De}\frac{\partial v}{\partial t}=-\frac{dp}{dx}+(1-s)\frac{\partial c_{12}}{\partial y}+s\frac{\partial^2 v}{\partial y^2}. \tag{3}$$

On the other hand, for the Leonov model we have

$$\frac{\partial c_{11}}{\partial t}-2\frac{\partial v}{\partial y}c_{12}+\frac{1}{2}({c_{11}}^2+{c_{12}}^2-1)=0,$$

$$\frac{\partial c_{22}}{\partial t}+\frac{1}{2}({c_{12}}^2+{c_{22}}^2-1)=0,$$

$$\frac{\partial c_{12}}{\partial t}-\frac{\partial v}{\partial y}c_{22}+\frac{1}{2}c_{12}(c_{11}+c_{22})=0,\ c_{33}=1,\ c_{13}=c_{23}=0,$$

$$\frac{Re}{De}\frac{\partial v}{\partial t}=-\frac{\partial p}{\partial x}+(1-s)\frac{\partial}{\partial y}\left[\left(\frac{I_1}{3}\right)^n c_{12}\right]+s\frac{\partial^2 v}{\partial y^2},$$

$$-\frac{\partial p}{\partial y}+(1-s)\frac{\partial}{\partial y}\left[\left(\frac{I_1}{3}\right)^n c_{22}\right]=0. \tag{4}$$

Here we have introduced the following dimensionless set of variables:

$$\frac{x_1}{H_0}=x,\ \frac{x_2}{H_0}=y,\ \frac{t}{\theta}\to t,\ \frac{\theta}{H_0}v_1=v,\ \frac{p}{G}\to p,\ Re=\frac{\rho UH_0}{G\theta},$$

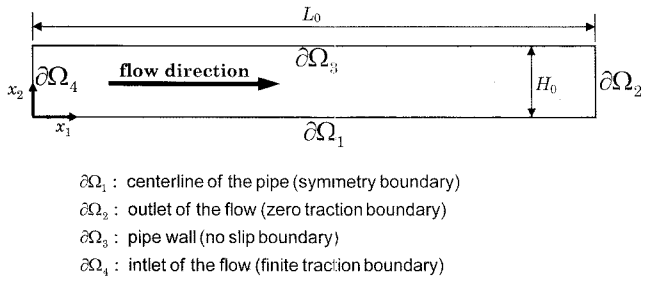

Fig. 1. Domain of the 1D and 2D problems in planar Poiseuille flow of viscoelastic liquid.

$$De = \frac{\theta U}{H_0}, \tag{5}$$

where H_0 is the half height of the flow channel depicted in Fig. 1, and U is some characteristic speed. The specification of U is meaningless in this work, since only the combination $\frac{Re}{De}$ appears in the equations. We also define the dimensionless average flowrate $\bar{v}$ as

$$\bar{v} = \int_0^1 v dy = \frac{\theta}{H_0^2}\int_0^{H_0} v_1 dx_2 . \tag{6}$$

At $t=0$, we apply finite constant pressure gradient $p_x = -\frac{\partial p}{\partial x}$=const. One can notice that for the Leonov model $\frac{\partial p}{\partial y} \neq 0$, whereas the pressure for the Oldroyd-B model is dependent only on x in the Poiseuille flow. In this sort of flow, the Oldroyd-B model generates an analytical solution, which has been first obtained by Waters and King (1970). We present another simple way of derivation of the same solution in the Appendix and the solutions for v and c_{12} are given in Eqs. (A.13) and (A.16), respectively. Eq. (A.14) expresses the average flowrate $\bar{v}$.

In this work, both constitutive models including the equations of motion and continuity are numerically approximated. We employ second order discretization schemes such as the Crank-Nicolson method for temporal and the central difference for spatial approximation. Since the analytical solutions are available for the Oldroyd-B model, the discrete solutions are compared with analytic ones to verify the accuracy of the current numerical scheme.

Employing the finite element analysis, we have already presented the direct 2D solution of viscoelastic Poiseuille flow under constant pressure difference between inlet and outlet of the pipe (Kwon, 2007). In that work, we implemented the traction boundary that specifies traction forces both at the inlet and outlet and the values of **c** tensor corresponding to the stationary state at the inlet. However in the case of inertial flow ($\rho \neq 0$), we are confronted with some deficiency of boundary information if we still intend to maintain boundary values of velocity as unknown in order to observe *e.g.* the fluctuation of the flowrate at flow start-up. While the equation of motion is an elliptic partial differential equation in inertialess flow, it becomes hyperbolic when the density or the Reynolds number is nonzero, and then the condition at the initial boundary of the velocity characteristic curves has to be assigned. On the other hand if we specify the velocity boundary values at the inlet, the traction value is no longer necessary. Thus one may assert that the solution of inertial viscoelastic flow with traction boundary is meaningless at all since the system of equations is in the lack of required data and becomes indeterminate. We consider and discuss this problem in more detail, comparing the 2D finite element solution with the 1D results.

3. Results and discussion

In all the results of this work, we have specified a small value for the retardation parameter such as $s=0.001$ in order to mainly examine elastic behavior of flow. However

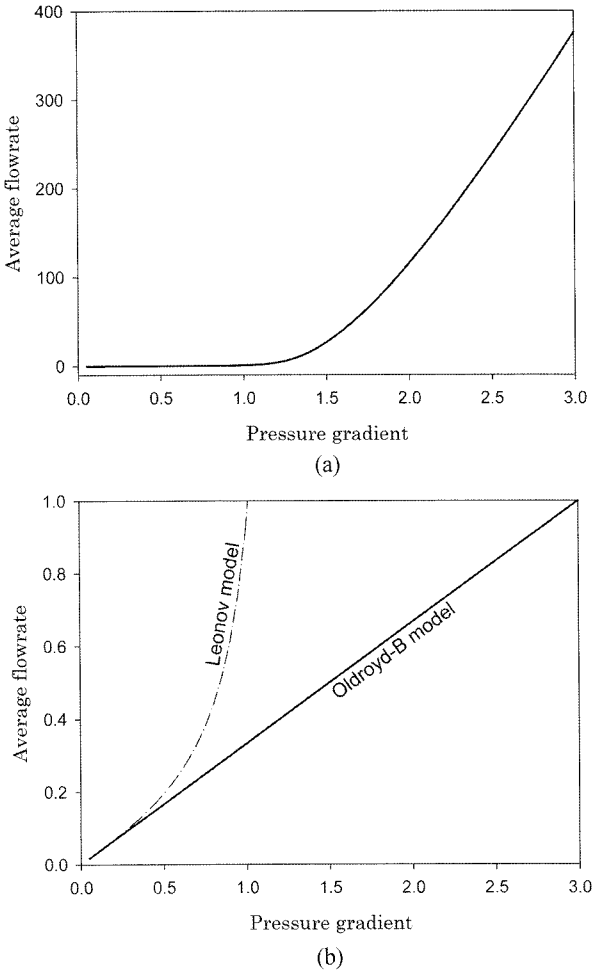

Fig. 2. Variation of steady average flowrate with pressure gradient. (a) Leonov model, (b) Oldroyd-B and Leonov models.

we cannot assign $s=0$ along with $\rho=0$ since this condition incurs infinite instantaneous flow speed due to pure elasticity at the moment of applying pressure difference between inlet and outlet of the channel. The Leonov constitutive equation contains one additional nonlinear parameter n which has to be positive for mathematical global stability (Kwon and Leonov, 1995), and here it is specified to be 0.1. All other parameters such as Re/De and $p_x \equiv -\frac{\partial p}{\partial x}$ are adjusted to examine their effects. We divide the gap H_0 into 100 discretized intervals that have been determined as the optimal number of elements according to numerical experiments. When obtaining the result, the criterion of convergence tolerance is set to be 10^{-4} in the L_∞ norm of relative residuals.

We first examine the steady result. Fig. 2 depicts the steady flowrate represented as a function of the pressure gradient p_x. The Oldroyd-B equation describes linear dependence of the flowrate due to its Newtonian characteristic of the shear viscosity. Both the models exhibit the same behavior in the case of small p_x, since they should show the same asymptotic linear viscoelastic behavior in the slow flow. However, due to shear thinning the curve corresponding to the Leonov equation displays severe upturn, that is, the decrease of viscosity at high shear.

In Fig. 3 one can observe the profile of steady axial velocity in the direction of channel height. All the dimensionless velocity values are again normalized by its value at the centerline. As is well known, the Oldroyd-B model demonstrates the Newtonian parabolic velocity profiles, all of which fall on the same curve. On the other hand, the Leonov constitutive equation describes typical shear thinning characteristic that the flat velocity profile appears away from the wall as the flowrate or the pressure gradient increases. Peculiarly the region of flat profile diminishes when p_x exceeds 2 probably due to relatively high shear

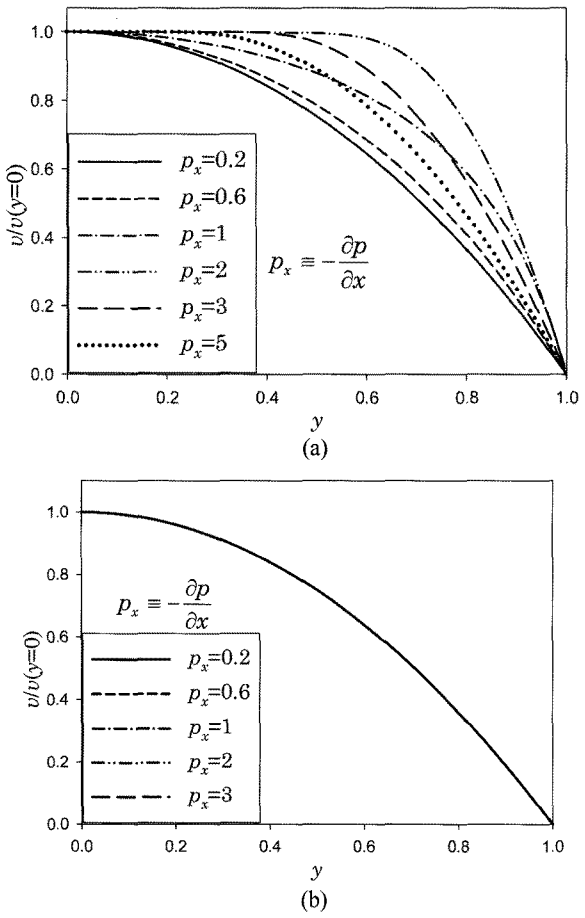

Fig. 3. Transverse directional profiles of steady axial velocity normalized in terms of the central speed at various pressure gradients. (a) Leonov model, (b) Oldroyd-B model.

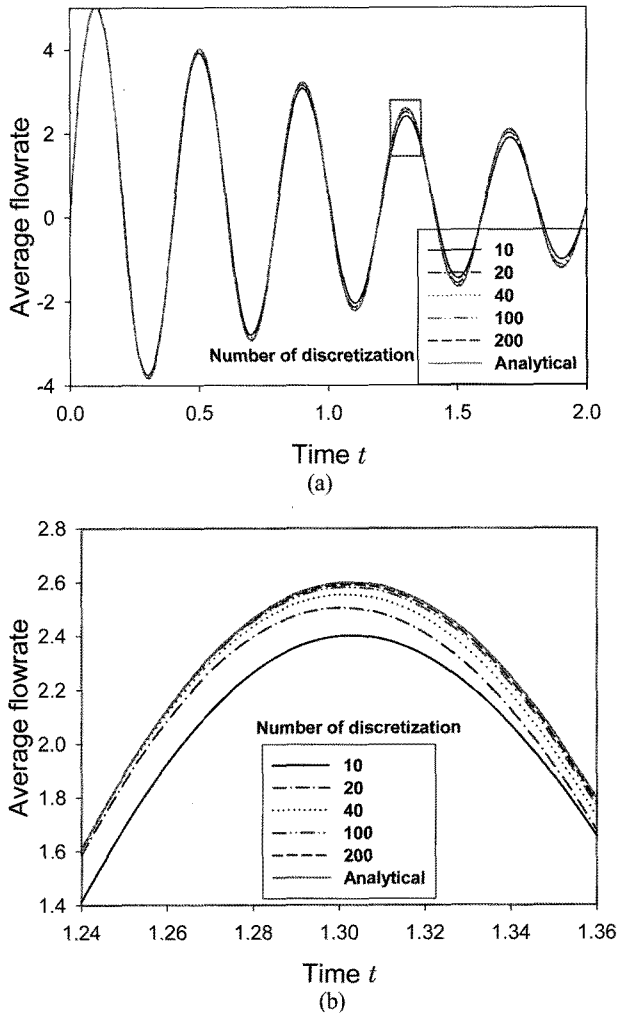

Fig. 4. (a) Comparison of the time evolution of average flowrate for various degree of spatial discretization with the analytical solution, (b) enlarged view of the square box in (a). (the Oldroyd-B model in planar Poiseuille flow under constant pressure gradient $p_x \equiv -\frac{\partial p}{\partial x} = 1$ with s=0.001 and density $\rho=0.01$, where ρ corresponds to Re/De).

rate away from the wall achieved at high p_x. It may be worth mentioning that (almost) analytical results can be obtained in steady Poiseuille flow for both models and the profiles in the figure are obtained from those results.

For the Oldroyd-B model, the comparison of numerical approximation with analytical solution is shown for various degree of spatial discretization in y-direction. Even though the time steps vary during the evolution of flowrate in order to enhance the speed of computation, for each calculation they are fixed to endow the same degree of accu-

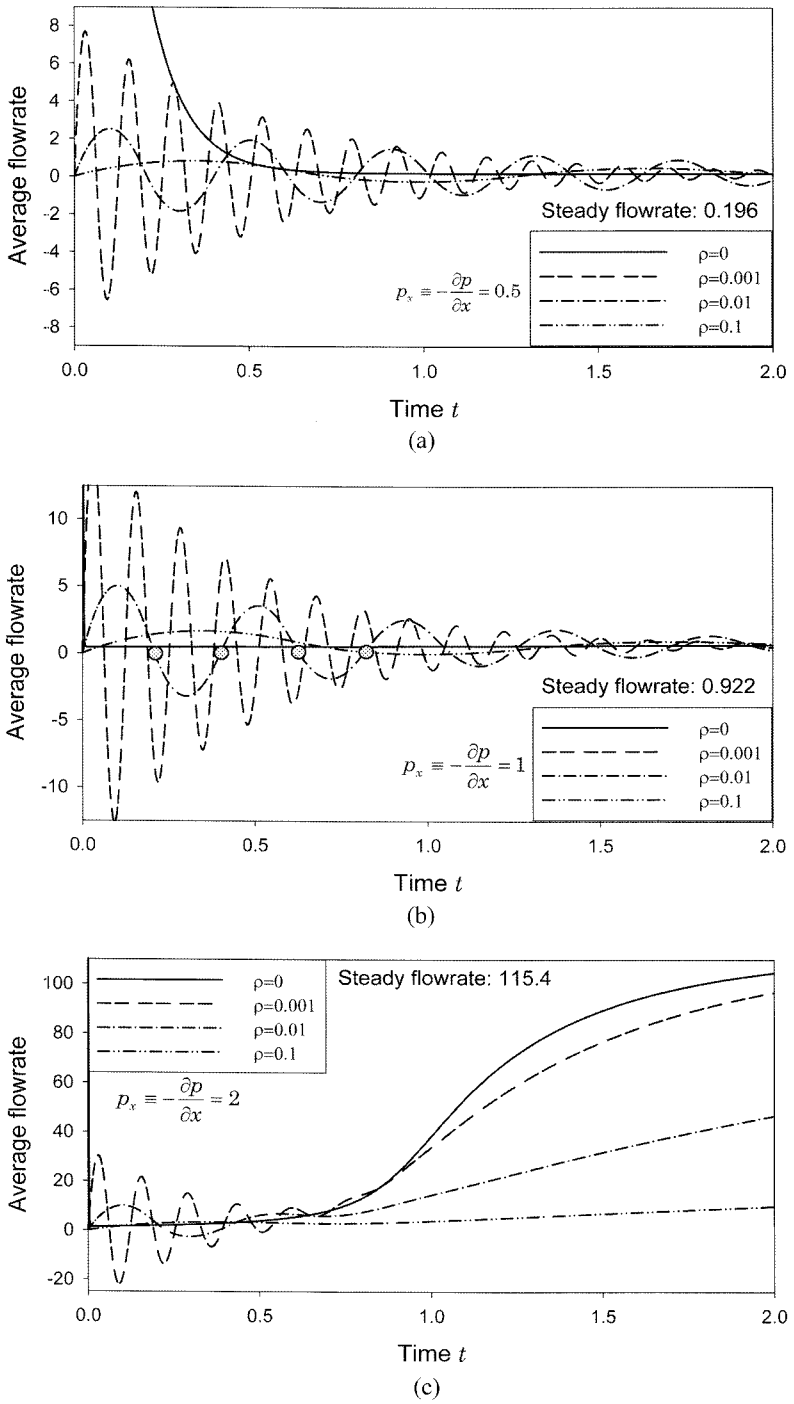

Fig. 5. Evolution of average flowrate for the Leonov model in planar Poiseuille flow under constant pressure gradient with various density ρ (Here ρ corresponds to *Re/De*).

(a) $p_x \equiv -\frac{\partial p}{\partial x} = 0.5$, (b) 1, (c) 2.

racy of temporal approximation. In the enlarged view of Fig. 4(b), one may conclude that the numerical solutions with 100 and 200 subintervals express the analytical solution quite accurately. Thus from this time on we fix the number of discrete spatial steps to be 100.

Figs. 5 and 6 illustrate the time evolution of the start-up flowrate for the Leonov and Oldroyd-B models, respectively. The variation of flowrate is shown for the Leonov model with respect to three different values of pressure gradient in Fig. 5 and for the Oldroyd-B model with two fixed p_x in Fig. 6. As can be easily seen from Eq. (3) or (4), at fixed p_x all the steady values coincide without regard to the value of the density which is here defined as the ratio of the Reynolds to Deborah number. In the case of inertialess flow, after the action of pressure the flowrate immediately reaches a finite value that corresponds to the value for the creeping Newtonian flow with viscosity $s\eta$, and then decays to its viscoelastic steady limit with some possible minor fluctuations. Such behavior is partially shown by the initial decrease of the solid line in Fig. 5(a). However such decreases in Figs. 5(b) and 5(c) are hidden due to its extreme rapidness at the initial stage, and only the later behavior has been shown as a horizontal solid line in Fig. 5(b) and gradually increasing solid curve in Fig. 5(c). When we assign no retardation in the constitutive equation, *i.e.*, $s=0$, the flowrate instantly reaches infinity at the moment of pressure application for the creeping flow.

In almost all cases of start-up viscoelastic flow with finite inertia for both models, the flowrate exhibits severe oscillation, that is, forward and even backward transitions in flow direction. Such flow reversal or oscillation is incurred by the competition between inertial and elastic forces. Certainly, the frequency of oscillation varies with density. In the case of asymptotic linear shear wave, the propagation speed may be determined by $\sqrt{G/\rho}$, which explains the reciprocal of wave frequency is proportional to $\sqrt{\rho}$. The inertial flow curves in Figs. 5(a)-(b) and 6 also express similar behavior that the wavelength of flowrate oscillation approximately increases with a proportionality constant $\sqrt{\rho}$. Somewhat more detailed discussion on this kind of flow oscillations for the Oldroyd-B model can be found in the work by Sato and Richardson (1994).

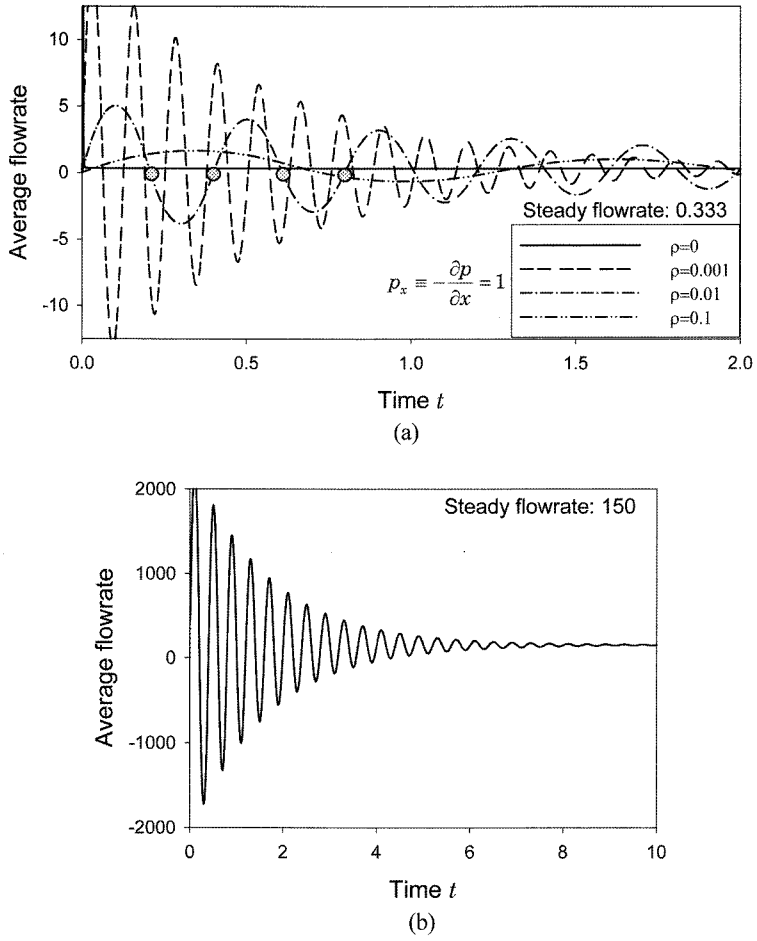

Fig. 6. Evolution of average flowrate for the Oldroyd-B model in planar Poiseuille flow under constant pressure gradient with various density ρ (Here ρ corresponds to *Re/De*). (a) $p_x \equiv -\frac{\partial p}{\partial x} = 1$, (b) 450.

The solution for the Oldroyd-B model illustrated in Fig. 6(a) qualitatively exhibits behavior similar to the corresponding one for the Leonov model in Fig. 5(b). However under the action of the same pressure gradient the steady value is lower due to the absence of shear thinning, and the transient behavior, that is, the flowrate oscillation seems to persist longer before fading out.

As the inertia of flow decreases, the initial amplitude of oscillations increases, but the asymptotic solution for $\rho \rightarrow 0$ does not seem to approach the solution for the inertialess flow. However at this point with these limited results of analysis, we cannot rush to draw any conclusion regarding the asymptotic behavior of solution.

One may examine qualitatively different behavior of the Leonov model at high pressure gradient represented in Fig. 5(c). In this high pressure application, the apparent average flowrate during initial flow oscillation is much lower than its eventual steady value 115.4, and then the flowrate gradually increases. This qualitative change with the increase of pressure gradient is graphically explained in Fig. 7. The time required to achieve the steady state is much longer than the previous case of lower pressure application. As the liquid density grows, this time of transient behavior also significantly increases. On the other hand, the Oldroyd-B model does not exhibit such drastic change of flow behavior as illustrated in Fig. 6(b). The applied pressure gradient is as high as 450 and the resultant steady flowrate becomes 150. However it simply demonstrates behavior qualitatively similar to the one at low flowrate even though the amplitude of oscillation dramatically increases to over 2000. This fundamental difference of flow behavior for corresponding constitutive equations may again result from the absence or presence of shear thinning.

Fig. 7 expresses time evolution of flowrate at $\rho=0.01$ for several values of pressure gradient. As previously mentioned, when the pressure gradient exceeds a certain value, the flowrate curve exposes qualitatively different transition. When p_x is 1.25 or higher, the steady value of flowrate starts to exceed the transient value during oscillations. The steady values for $p_x=1.25$ and 1.5 are 5.56 and 26.6, respectively. It seems that the period of oscillation slightly increases with p_x.

In Figs. 8 and 9 the time variations of axial velocity profiles near the moments of initial 4 flow reversals (those moments are denoted in Figs. 5(b) and 6(a) with small circles) are presented for the Leonov and Oldroyd-B models. In all the figures the time interval between successive curves is 0.005. When the flow changes its direction from forward to backward in Figs. 8(a) and 9(a), the retracting flow speed (that is, for the lowest curve in both figures) becomes higher near the wall ($y \approx 0.65$) than that near the center ($y \approx 0$). This may imply that recovery originating from the elasticity accumulated during the forward flow is higher near the wall than that near the center. This can be understood from the corresponding higher value of shear rate near the wall, and thus the recovery results from the higher wall shear. From the magnitude of total variation of curves with time, one can again observe decay of flow oscillations for the Leonov model faster than that for the Oldroyd-B model, which means faster dissipation exhibited by the Leonov model at the same values of parameters s and ρ.

One can observe the comparison of the result in this work with the previous one computed in terms of 2D finite element analysis. The detail of the 2D computation scheme has already been given in Kwon (2007). In that study, so called the traction boundary has been specified to achieve viscoelastic flow under the action of pressure difference Δp, that is, the difference of pressures at the inlet and outlet. Therefore the average pressure gradient is considered as $\Delta p/L_0$, where $L_0=10H_0$ in the computation. Due to the hyperbolicity of the evolution equation of **c**, at the flow

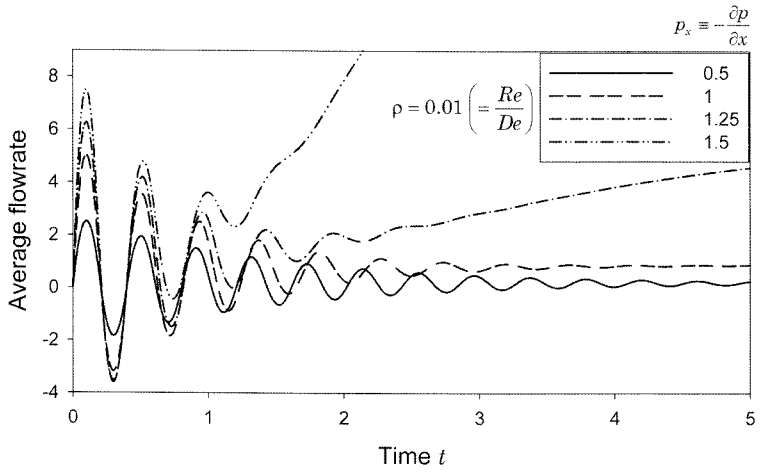

Fig. 7. Evolution of average flowrate for the Leonov model in planar Poiseuille flow under various constant pressure gradients at density $\rho=0.01$.

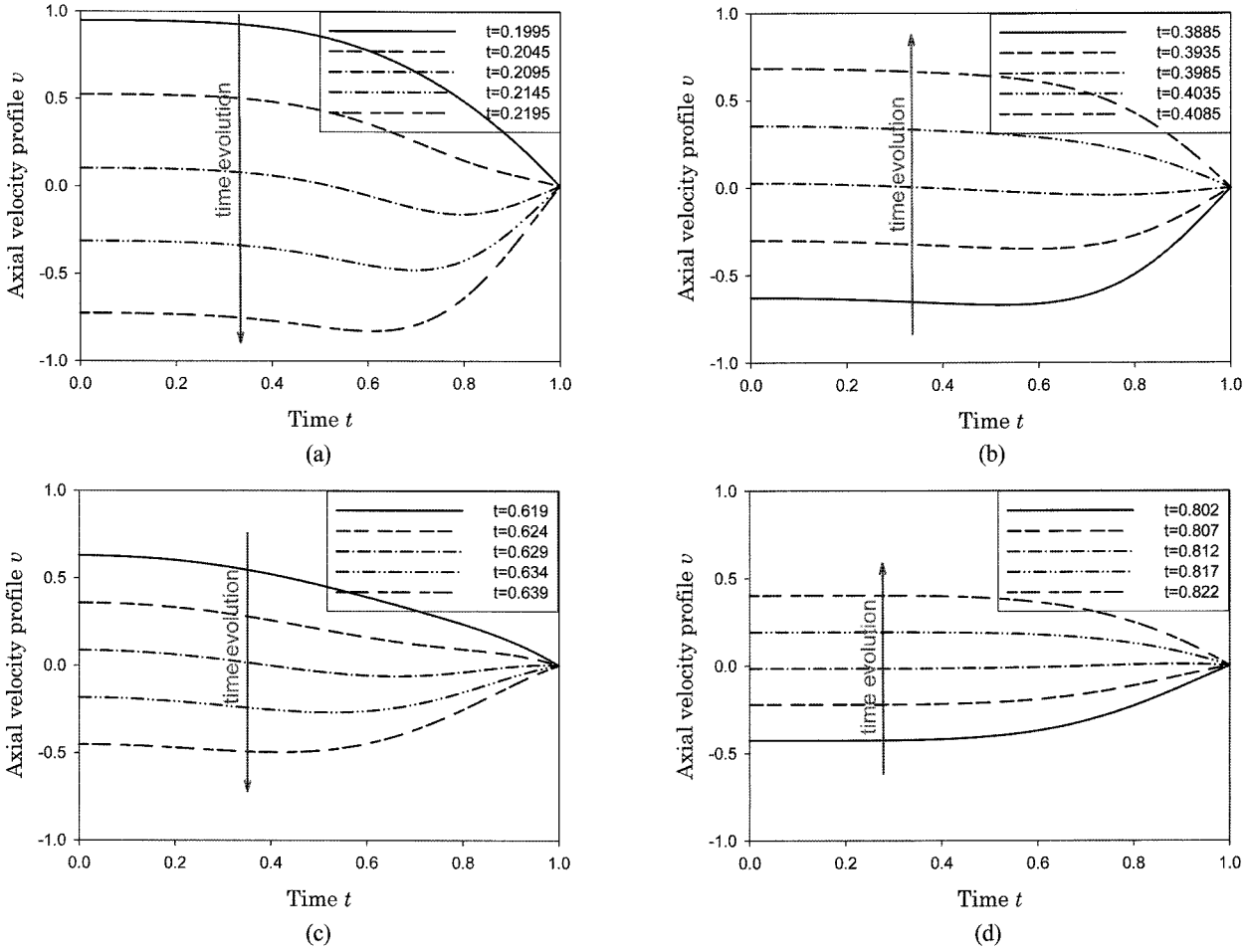

Fig. 8. Axial velocity profiles at the moments of flow reversal for the Leonov model with $\rho=0.01$ and $p_x=1$. (a) $t\approx0.2$, (b) 0.4, (c) 0.6, (d) 0.8.

inlet we have to assign the boundary values of **c** which are unknown and therefore its stationary value δ has been assigned. These boundary conditions of traction forces and $\mathbf{c}=\delta$ do not induce simple 1D but 2D flow patterns near the inlet and outlet even in the steady state.

In Fig. 10 for $\rho=0.01$, 0.001 and the pressure gradient of 0.5 (p_x for 1D and $\Delta p/L_0$ for 2D calculation), the time variation of flow rate is illustrated for both computation schemes. Even though the overall behavior of solutions coincides well, one can still examine the difference between 2 approaches. Especially somewhat retarded oscillation of the flowrate in 2D computation can be clearly seen. In 1D modeling, we automatically assume that the flow is fully developed or equivalently the channel is infinitely long. Due to the 2D flow characteristic explained in the previous paragraph with finite channel length $L_0=10H_0$, the assumption of fully developed flow is certainly invalid in the whole domain of finite element computation. Therefore this results in the discrepancy of solutions of 2 different computation schemes. In addition, such complex 2D flow rearrangement, one example of which is portrayed in Fig. 11, procrastinates the procedure of flow reversal or flowrate fluctuation exhibited in Fig. 10. In Fig. 11, it can be distinctly seen that the fully developed flow approximation seems valid only in the middle region of the channel.

Before concluding this report, it is worth mentioning one mathematical point in 2D finite element analysis of viscoelastic flow under pressure difference with finite inertia. In the case of inertialess (creeping) flow approximation, the equation of motion constitutes a set of elliptic partial differential equations. However in the inertial flow with finite density ($\rho\neq0$) it suddenly changes its type to hyperbolic equations, where one requires additional boundary condition of velocity at the flow inlet (or the initial condition at the starting point of characteristic curves). In this case of finite inertia, the traction boundary condition assigned in order to examine flow fluctuations loses its validity and thus applicability, and with velocity assigned as boundary conditions the flowrate is not unknown any more especially in the incompressible flow. In other words, one can no more investigate the flowrate variation of iner-

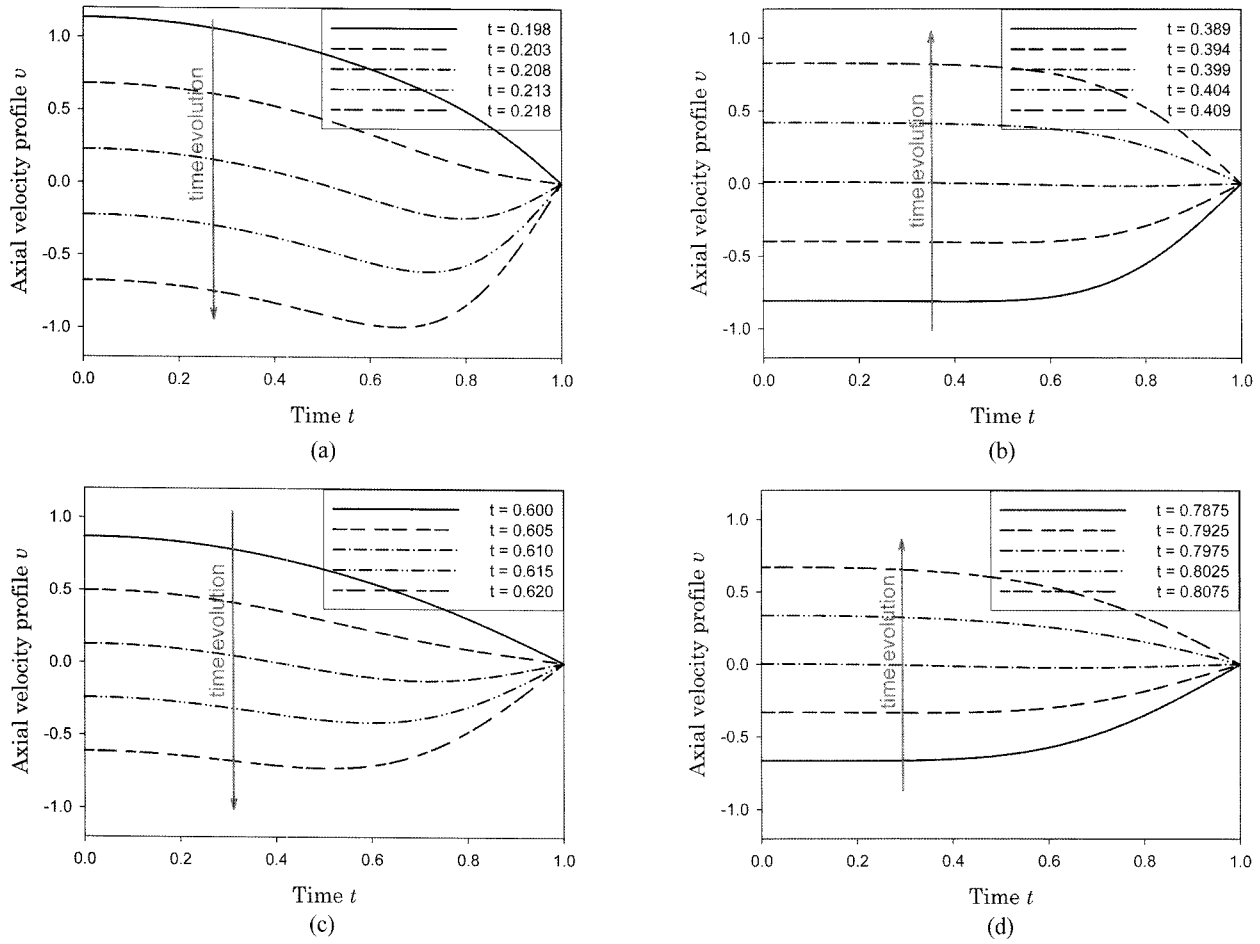

Fig. 9. Axial velocity profiles at the moments of flow reversal for the Oldroyd-B model with $\rho=0.01$ and $p_x=1$. (a) $t\approx 0.2$, (b) 0.4, (c) 0.6, (d) 0.8.

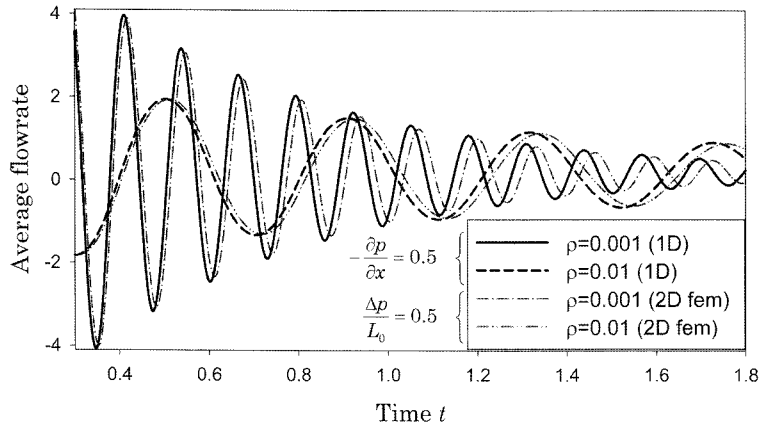

Fig. 10. Comparison of 1D and 2D computations for the time evolution of flowrate in planar Poiseuille flow of the Leonov model. In the case of 1D computation, $p_x \equiv -\frac{\partial p}{\partial x} = 0.5$ and in the case of 2D finite element analysis, $\frac{\Delta p}{L_0} = 0.5$.

tial flow under finite pressure difference.

In the previous 2D computation (Kwon, 2007), the partial result of which is also introduced in this work for comparison, we have left the inlet boundary value of velocity unknown, that is, we have solved an undetermined set of equations in 2D inertial viscoelastic flow problems.

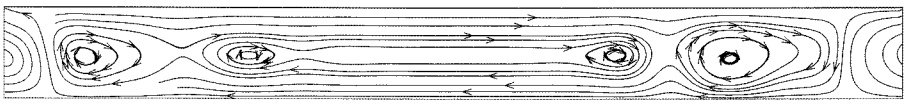

$t = 0.405,\ \bar{v} = -0.0028$

Fig. 11. Complex behavior of streamlines at the moment of flow reversal (t=0.405) described by 2D finite element analysis under finite pressure difference with ρ=0.01 and $\frac{\Delta p}{L_0} = 0.5$ (Kwon, 2007).

Although we managed to attain a stable computation, the solution obtained may not have scientific meaning. However via the comparison in this work with 1D modeling, we may assert validity of 2D finite element solutions since it shows reasonable coincidence between 2 results and also demonstrates difference that can be explained with logical reasoning. In the 2D study (Kwon, 2007) we were not able to achieve stable computation at high pressure difference probably due to the lack of boundary condition for inlet velocity.

4. Conclusions

We have investigated the transient behavior of 1D fully developed Poiseuille viscoelastic flow under finite pressure gradient expressed by the Oldroyd-B and Leonov constitutive equations. Both models demonstrate qualitatively similar solutions at low pressure gradient, but their eventual steady flowrate exhibits noticeable difference due to Newtonian shear or shear thinning behavior. In the inertialess flow, the flowrate instantaneously attains a large value corresponding to the Newtonian creeping flow and then decreases to its steady value with minor fluctuations when the applied pressure gradient is low. However with finite liquid density the flow shows severe fluctuation with reversals of flow directions, which sustains for a quite long period before reaching steady state. The qualitative difference between two constitutive equations from the view point of description of flow behavior has been examined. For the Leonov model as the assigned pressure gradient increases, the flowrate achieves its steady value significantly higher than its value during oscillations and the time required for steady state also remarkably increases for both creeping and inertial flows. We have also illustrated difference as well as similarity between 1D and 2D results and possible mechanism of complex 2D flow rearrangement employing a solution of previous finite element computation.

Acknowledgements

This study was supported by research grants from the Korea Science and Engineering Foundation (KOSEF) through the Applied Rheology Center (ARC), an official KOSEF-created engineering research center (ERC) at Korea University, Seoul, Korea.

Appendix

Employing the Laplace transform and contour integrals on the complex plane, Waters and King (1970) have already provided the analytical solution for the planar Poiseuille flow of the Oldroyd-B fluid. Here we revisit this problem and present a simpler solution procedure that implements routine method of variable separation and some physical reasoning for missing initial condition.

The Oldroyd-B constitutive equation (2) with equations of motion and continuity (1) yields the dimensionless set (3) of equations, which is rewritten as

$$\frac{\partial c_{11}}{\partial t} - 2\frac{\partial v}{\partial y}c_{12} + c_{11} - 1 = 0,\ \frac{\partial c_{12}}{\partial t} - \frac{\partial v}{\partial y} + c_{12} = 0,\ c_{22} = c_{33} = 1,$$

$$c_{13} = c_{23} = 0,\ \frac{Re}{De}\frac{\partial v}{\partial t} = p_x + (1-s)\frac{\partial c_{12}}{\partial y} + s\frac{\partial^2 v}{\partial y^2},\ p_x = -\frac{dp}{dx}. \quad \text{(A.1)}$$

Here the following initial and boundary conditions are supplemented:

$$c_{11}(t=0) = c_{11}(y=0) = 1,\ c_{12}(t=0) = c_{12}(y=0) = 0,$$

$$v(t=0) = \frac{\partial v}{\partial y}(y=0) = v(y=1) = 0.$$

Again the dimensionless group same with the previous set (5) is employed.

The corresponding steady solution becomes

$$v^s = \frac{p_x}{2}(1-y^2),\ c_{11}^s = 1 + 2p_x^2 y^2,\ c_{12}^s = -p_x y. \quad \text{(A.2)}$$

To simplify the given set of equations, we introduce

$$u = v - v^s,\ d_{11} = c_{11} - c_{11}^s,\ d_{12} = c_{12} - c_{12}^s. \quad \text{(A.3)}$$

Then we have

$$\frac{\partial d_{11}}{\partial t} + 2p_x y\left(\frac{\partial u}{\partial y} + d_{12}\right) - 2\frac{\partial u}{\partial y}d_{12} + d_{11} = 0,$$

$$\frac{\partial d_{12}}{\partial t} - \frac{\partial u}{\partial y} + d_{12} = 0,$$

$$\frac{Re}{De}\frac{\partial u}{\partial y} = (1-s)\frac{\partial d_{12}}{\partial y} + s\frac{\partial^2 u}{\partial y^2}. \quad \text{(A.4)}$$

From the second and the third of Eqs. (A.4) one can obtain

$$\frac{Re}{De}\left(\frac{\partial^2 u}{\partial t^2}+\frac{\partial u}{\partial t}\right)=\frac{\partial^2 u}{\partial y^2}+s\frac{\partial^3 u}{\partial t\partial y^2}. \quad (A.5)$$

Now the routine method of variable separation to solve the above partial differential equation may be applied by setting $u(t,y)\equiv U(t)\Gamma(y)$, which results in

$$\frac{Re}{De}(U''+U')\Gamma=(U+sU')\Gamma'' \text{ or}$$

$$\frac{Re}{De}\frac{U''+U'}{U+sU'}=\frac{\Gamma''}{\Gamma}=-\lambda^2, \quad (A.6)$$

where U', U'', Γ', Γ'' are the first and second derivatives of U and Γ with respect to corresponding variables and λ^2 assigns nonnegative eigenvalues of the system. Since we are given with the boundary condition $\Gamma(1)=\Gamma'(0)=0$, the spatial dependence is expressed as

$$\Gamma_n(y)=\cos(\lambda_n y),\ \lambda_n=\left(n-\frac{1}{2}\right)\pi,\ n=1,2,3,\cdots. \quad (A.7)$$

For the temporal dependence, the ordinary differential equation yields

$$U_n(t)=A_n e^{-\kappa_n t}[\cosh(t\sqrt{\kappa_n^2-\mu_n})+B_n\sinh(t\sqrt{\kappa_n^2-\mu_n})], \quad (A.8)$$

where $\mu_n=\frac{De}{Re}\lambda_n^2$, $\kappa_n=\frac{1}{2}(1+s\mu_n)$ and A_n and B_n are constants to be determined from the initial conditions. Combination of the results (A.7) and (A.8) with (A.3) gives

$$v=\frac{P_x}{2}(1-y^2) + \sum_{n=1}^{\infty} A_n\cos(\lambda_n y)e^{-\kappa_n t}[\cosh(t\sqrt{\kappa_n^2-\mu_n})+B_n\sinh(t\sqrt{\kappa_n^2-\mu_n})]. \quad (A.9)$$

We are able to specify A_n employing the initial condition $v(t=0)=0$ such that

$$A_n=-p_x\int_0^1(1-y^2)\cos(\lambda_n y)dy=\frac{2p_x}{\lambda_n^3}(-1)^n. \quad (A.10)$$

Even though an additional condition that permits to determine B_n is absent, we may utilize physical reasoning that possibly introduces the missing requirement. The solution represented in Eq. (A.9) should asymptotically coincide with the solution for the Newtonian flow with viscosity $s\eta$ at $t=0+$, which can be easily obtained for the corresponding differential equation $\frac{Re}{De}\frac{\partial v^{Newton}}{\partial t}=p_x+s\frac{\partial^2 v^{Newton}}{\partial y^2}$ with conditions $v^{Newton}(t=0)=\frac{\partial v^{Newton}}{\partial y}(y=0)=v^{Newton}(y=1)=0$. Employing the similar but much simpler procedure results in

$$v^{Newton}=\frac{p_x}{s}\left\{\frac{1}{2}(1-y^2)+2\sum_{n=1}^{\infty}\frac{(-1)^n}{\lambda_n^3}\cos(\lambda_n y)e^{-s\mu_n t}\right\}. \quad (A.11)$$

Thus the application of the following observation

$$\frac{\partial v}{\partial t}(t=0+)=\frac{\partial v^{Newton}}{\partial t}(t=0+)=-2p_x\sum_{n=1}^{\infty}\frac{(-1)^n}{\lambda_n^3}\mu_n\cos(\lambda_n y),$$

eventually produces

$$B_n=\frac{\kappa_n-\mu_n}{\sqrt{\kappa_n^2-\mu_n}}. \quad (A.12)$$

Then we have

$$v=p_x\left\{\frac{1}{2}(1-y^2) +2\sum_{n=1}^{\infty}\frac{(-1)^n}{\lambda_n^3}\cos(\lambda_n y)e^{-\kappa_n t}\left[\cosh(t\sqrt{\kappa_n^2-\mu_n})+\frac{\kappa_n-\mu_n}{\sqrt{\kappa_n^2-\mu_n}}\sinh(t\sqrt{\kappa_n^2-\mu_n})\right]\right\} \quad (A.13)$$

Accordingly the average flowrate is derived as

$$\bar{v}\equiv\int_0^1 v\,dy=p_x\left\{\frac{1}{3}-2\sum_{n=1}^{\infty}\frac{1}{\lambda_n^4}e^{-\kappa_n t}\left[\cosh(t\sqrt{\kappa_n^2-\mu_n})+\frac{\kappa_n-\mu_n}{\sqrt{\kappa_n^2-\mu_n}}\sinh(t\sqrt{\kappa_n^2-\mu_n})\right]\right\} \quad (A.14)$$

Eq. (A.13) exactly coincides with the result first obtained by Waters and King (1970).

Substitution of Eq. (A.13) into the second of Eq. (A.4) results in

$$\frac{\partial d_{12}}{\partial t}+d_{12}=-2p_x\sum_{n=1}^{\infty}\frac{(-1)^n}{\lambda_n^2}\sin(\lambda_n y)e^{-\kappa_n t}\left[\cosh(t\sqrt{\kappa_n^2-\mu_n})+\frac{\kappa_n-\mu_n}{\sqrt{\kappa_n^2-\mu_n}}\sinh(t\sqrt{\kappa_n^2-\mu_n})\right]. \quad (A.15)$$

This can be easily solved as

$$d_{12}=G(y)e^{-t}-2p_x\sum_{n=1}^{\infty}\frac{(-1)^n}{\lambda_n^2}\sin(\lambda_n y)e^{-\kappa_n t} \times\left[\cosh(t\sqrt{\kappa_n^2-\mu_n})+\frac{\kappa_n}{\sqrt{\kappa_n^2-\mu_n}}\sinh(t\sqrt{\kappa_n^2-\mu_n})\right]$$

or

$$c_{12}=-p_x y+G(y)e^{-t}-2p_x\sum_{n=1}^{\infty}\frac{(-1)^n}{\lambda_n^2}\sin(\lambda_n y)e^{-\kappa_n t} \times\left[\cosh(t\sqrt{\kappa_n^2-\mu_n})+\frac{\kappa_n}{\sqrt{\kappa_n^2-\mu_n}}\sinh(t\sqrt{\kappa_n^2-\mu_n})\right],$$

where $G(y)$ is the integration constant (a function of y) that has to be determined from the initial condition. The initial condition $c_{12}(t=0)=0$ and the relation $2\sum_{n=1}^{\infty}\frac{(-1)^n}{\lambda_n^2}\sin(\lambda_n y)$

$=-y$ that may be obtained from the initial condition for v and its differentiation with respect to y, simply yield $G(y)=0$. Therefore we have

$$c_{12}=-p_x y-2p_x\sum_{n=1}^{\infty}\frac{(-1)^n}{\lambda_n^2}\sin(\lambda_n y)e^{-\kappa_n t}$$

$$\times\left[\cosh(t\sqrt{\kappa_n^2-\mu_n})+\frac{\kappa_n}{\sqrt{\kappa_n^2-\mu_n}}\sinh(t\sqrt{\kappa_n^2-\mu_n})\right] \qquad \text{(A.16)}$$

With Eqs. (A.13) and (A.16) the relation $\tau_{12}=(1-s)c_{12}+s\frac{\partial v}{\partial y}$ simply expresses the total dimensionless shear stress scaled by G. In Eqs. (A.13-16), the hyperbolic cosine and sine functions have to be substituted by the corresponding cosine and sine functions when $\kappa_n^2-\mu_n$ becomes negative.

In a similar way, we may represent the normal component c_{11} as

$$c_{11}=1+2e^{-t}\int_0^t e^{t'}\frac{\partial v(t,y)}{\partial y}c_{12}(t,y)dt\,. \qquad \text{(A.17)}$$

Thus the analytical expression can readily be obtained. However in this work, we have not made an attempt to obtain concrete expression of c_{11} or τ_{11} due to its unnecessariness as well as the awkwardness of the equation.

References

Duarte, A. S. R., A. I. P. Miranda and P. J. Oliveira, 2008, Numerical and analytical modeling of unsteady viscoelastic flows: The start-up and pulsating test case problems, *J. Non-Newton. Fluid Mech.* **154**, 153-169.

Fyrillas, M. M., G. C. Georgious and D. Vlassopoulos, 1999, Time-dependent plane Poiseuille flow of a Johnson-Segalman fluid, *J. Non-Newton. Fluid Mech.* **82**, 105-123.

Kwon, Y and A. I. Leonov, 1995, Stability constraints in the formulation of viscoelastic constitutive equations, *J. Non-Newton. Fluid Mech.* **58**, 25-46.

Kwon, Y, 2007, Numerical result of complex quick time behavior of viscoelastic fluids in flow domains with traction boundaries, *Korea-Australia Rheology J.* **19**, 211-219.

Leonov, A. I., 1976, Nonequilibrium thermodynamics and rheology of viscoelastic polymer media, *Rheol. Acta* 15, 85-98.

van Os, R. G. M. and T. N. Phillips, 2004, Spectral element methods for transient viscoelastic flow problems, *J. Comp. Physics* **201**, 286-314.

Sato, T. and S. M. Richardson, 1994, Explicit numerical simulation of time-dependent viscoelastic flow problems by a finite element/finite volume method, *J. Non-Newton. Fluid Mech.* **51**, 249-275.

Tanner, R. I. and S. –C. Xue, 2002, Computing transient flows with high elasticity, *Korea-Australia Rheology J.* **14**, 143-159.

Waters, N. D. and M. J. King, 1970, Unsteady flow of an elastic-viscous liquid, *Rheol. Acta* **9**, 345-355.

Xue, S. –C., R. I. Tanner and N. Phan-Thien, 2004, Numerical modeling of transient viscoelastic flows, *J. Non-Newton. Fluid Mech.* **123**, 33-58.